

Measuring Atmospheric Carbon Dioxide from Space with the Orbiting Carbon Observatory-2 (OCO-2)

D. Crisp for the OCO-2 Team

Jet Propulsion Laboratory/California Institute of Technology, 4800 Oak Grove Drive, Pasadena, CA, USA 91109-8099

ABSTRACT

The Orbiting Carbon Observatory-2 (OCO-2) is this first NASA satellite designed to measure atmospheric carbon dioxide (CO_2) with the accuracy, resolution, and coverage needed to detect CO_2 sources and sinks on regional scales over the globe. OCO-2 was launched from Vandenberg Air Force Base on 2 July 2014, and joined the 705 km Afternoon Constellation a month later. Its primary instrument, a 3-channel imaging grating spectrometer, was then cooled to its operating temperatures and began collecting about one million soundings over the sunlit hemisphere each day. As expected, about 13% of these measurements are sufficiently cloud free to yield full-column estimates of the column-averaged atmospheric CO_2 dry air mole fraction, X_{CO_2} . After almost a full year in orbit, the X_{CO_2} product is beginning to reveal some of the most robust features of the atmospheric carbon cycle, including the northern hemisphere spring drawdown, and enhanced values co-located with intense fossil fuel and biomass burning emissions. As the carbon cycle science community continues to analyze these OCO-2 data, information on regional-scale sources (emitters) and sinks (absorbers) as well as far more subtle features are expected to emerge from this high resolution, global data set.

Keywords: Carbon Dioxide, CO_2 , Remote Sensing, Orbiting Carbon Observatory-2, OCO-2

1. INTRODUCTION

Human activities including fossil fuel combustion, cement production, and deforestation have increased the atmospheric CO_2 concentration by more than 40% since the beginning of the industrial age [1]. A quarter of this increase has been added since 2000 and the rate continues to accelerate. Fossil fuel combustion is the single largest source of CO_2 emissions. Until recently, most of these emissions originated from the industrialized world, where there are good records of the amount of fossil fuel burned. However, in 2007, China surpassed the U.S. as the single largest emitter of CO_2 , and the developing world now accounts for about 60% of all CO_2 emissions. The best existing inventories indicate that fossil fuel combustion and other human activities are now about 40 billion tons of CO_2 to the atmosphere each year, but the uncertainties on these estimates are growing almost as rapidly as the emissions themselves.

If all of the CO_2 emitted by these human sources remained in the atmosphere, the atmospheric CO_2 concentration would increase by more than one percent (1%) per year. Interestingly, precise measurements from a global network of greenhouse gas monitoring stations indicate that less than half of this CO_2 is remaining airborne. The rest is apparently being absorbed by natural *sinks* in the ocean and land biosphere, whose identity, and location are poorly understood. Roughly one quarter of the CO_2 emitted by human activities is apparently being absorbed by the ocean, where they contribute to ocean acidification. The land-based processes responsible for absorbing the other quarter of these emissions are far more mysterious. Some studies have attributed this absorption to tropical, mid-latitude, or boreal forests, while other indicate that these forest are just as likely to be net sources as sinks of CO_2 . The efficiency of these natural land and ocean sinks also appears to vary dramatically from year to year. Some years, they absorb almost all of the CO_2 emitted by human activities, while in other years, they absorb very little. The causes for this variability are not yet known. Because the identity, location, and processes controlling these natural sinks is not well understood, it is not possible to determine how much longer they will continue to reduce the rate of atmospheric CO_2 buildup by half. This lack of understanding introduces a major source of uncertainty in predictions of the rate of future CO_2 increases, and their effect on the climate. Measurements from the ground based greenhouse gas network accurately track the global atmospheric CO_2 budget and its trends, but do not have the resolution or coverage needed to identify the *sources* emitting CO_2 into the atmosphere or the natural *sinks* absorbing this gas at the Earth's surface. This information is critical to any carbon management strategy.

One way to improve the spatial and temporal sampling of CO₂ is to retrieve precise, spatially-resolved, global estimates of the column-averaged CO₂ dry air mole fraction (X_{CO_2}) from space. Surface weighted X_{CO_2} estimates can be retrieved from high resolution spectroscopic observations of reflected sunlight in near infrared CO₂ and O₂ bands. This is a challenging space based remote sensing observation because even the largest CO₂ sources and sinks produce changes in the background X_{CO_2} distribution no larger than 2%, and most are smaller than 0.25% (1 part per million (ppm) out of the background 400 ppm) [2]. The European Space Agency (ESA) EnviSat SCanning Imaging Absorption SpectroMeter for Atmospheric CHartographY (SCIAMACHY) [3] and Japanese Greenhouse Gases Observing Satellite (GOSAT) Thermal And Near infrared Sensor for carbon Observation Fourier Transform Spectrometer (TANSO-FTS) [4] were the first satellite instruments designed to exploit this measurement approach. SCIAMACHY collected column averaged CO₂ and methane (X_{CH_4}) measurements over the sunlit hemisphere from 2002 to 2012. TANSO-FTS has been collecting X_{CO_2} and X_{CH_4} observations since April 2009. These data have provided an excellent proof of concept, and are beginning to yield new insights into the carbon cycle, but improvements in sensitivity, resolution, and coverage are still needed.

2. THE ORBITING CARBON OBSERVATORY-2

The Orbiting Carbon Observatory-2 (OCO-2) is NASA's first satellite designed to measure atmospheric CO₂ with the accuracy, resolution, and coverage needed to detect CO₂ sources and sinks on regional scales over the globe. OCO-2 is a "carbon copy" of the Orbiting Carbon Observatory [5, 6], which was lost in 2009, when its launch vehicle malfunctioned and failed to reach orbit. OCO-2 carries and points a 3-channel, imaging, grating spectrometer. This instrument collects high resolution spectra of reflected sunlight in the 0.765 μm O₂ A-band and in the 1.61 and 2.06 μm CO₂ bands with unprecedented sensitivity. Coincident measurements from the three channels are combined into "soundings" that are analysed with a "full-physics" retrieval algorithm to yield estimates of X_{CO_2} and other geophysical quantities.

OCO-2 was successfully launched from Vandenberg Air Force Base in California on 2 July 2014. After completing a series of spacecraft check-out activities and orbit raising maneuvers, it joined the 705 km Afternoon Constellation (A-Train) on August 3, 2014. The optical bench and focal planes of the OCO-2 three-channel imaging grating spectrometer were then cooled to their operating temperatures and a series of calibration and validation activities was initiated. Since early September of 2014, this instrument has been routinely returning almost one million soundings each day over the sunlit hemisphere. Optically thick clouds and aerosols preclude observations of the full atmospheric column, but around 13% of these soundings are sufficiently cloud free to yield full-column estimates of X_{CO_2} with single-sounding random errors between 0.5 and 1 ppm at solar zenith angles as large as 70 degrees, as expected. These data are currently being analyzed by the OCO-2 Science Team and other members of the carbon cycle science community to assess their impact on our understanding of CO₂ sources and sinks on regional scales over the globe.

3. RETRIEVING X_{CO_2} AND SURFACE PRESSURE FROM REMOTE SENSING OBSERVATIONS OF REFLECTED SUNLIGHT

The Column averaged dry air mole fraction, X_{CO_2} , is defined as the ratio of the "column abundance" of CO₂ (i.e. the altitude-dependent CO₂ number density integrated over the atmospheric column) and the column abundance of "dry air." Surface weighted estimates of the column abundance of CO₂ can be retrieved from high resolution spectra of reflected sunlight in shortwave infrared (SWIR) CO₂ absorption bands [3, 4, 7, 8]. Similarly, estimates of the dry air column abundance can be inferred from spectra of near infrared (NIR) molecular oxygen (O₂) absorption bands. O₂ provides an ideal proxy for dry air because the mole fraction of oxygen in dry air is well known (0.20935) and essentially constant. Given this information, X_{CO_2} is defined as:

$$X_{CO_2} = 0.20935 \int N_{CO_2} ds / \int N_{O_2} ds . \quad (1)$$

Here, N_{CO_2} is the number density of CO₂ molecules, N_{O_2} is the number density of molecular oxygen, s is optical path length, and the integrals are performed over the atmospheric "column" extending from the sun, to the surface, to the spacecraft.

To estimate the column abundance of CO₂, the OCO-2 spectrometers collect co-bore-sighted measurements of reflected sunlight in the SWIR CO₂ bands centered near 1.61 and 2.06 μm . Co-bore-sighted measurements of the absorption of sunlight by the O₂ A-band near 0.765 μm are used for defining the total dry air column abundance. Measurements within the O₂ A-band and 2.06 μm CO₂ band also yield information about the vertical distribution and optical properties of optically thin clouds and aerosols along the optical path, reducing uncertainties in the optical path length associated with

scattering by these airborne particles. Water vapor absorption lines within the spectral regions sampled for the 1.61 and 2.06 μm channels provide the information needed to estimate the water vapor column abundance. These water vapor estimates are combined with the O_2 estimates from the A-band to derive the surface pressure. Temperature dependent CO_2 lines in the 2.06 μm region provide constraints on the atmospheric temperatures.

The remote sensing retrieval algorithm used to estimate X_{CO_2} and other geophysical quantities from the OCO-2 observations integrates a “full-physics” forward radiative transfer algorithm, a model of the optical throughput of the OCO-2 spectrometers, and an inverse method based on Bayesian Optical Estimation [7]. This algorithm performs a simultaneous retrieval using all 3 spectral bands and returns estimates of over 60 atmospheric and surface state properties. Its performance has been validated extensively using data from the Japanese GOSAT mission [7, 8], and has since been adapted for OCO-2 soundings.

4. THE OCO-2 INSTRUMENT

As noted above, the OCO-2 instrument incorporates three, co-boresighted, long-slit, imaging grating spectrometers optimized for observing the molecular oxygen (O_2) A-band at 0.765 microns (μm) and the carbon dioxide (CO_2) bands at 1.61 and 2.06 μm [6]. The three spectrometers use similar optical designs and are integrated into a common optical bench to improve system rigidity and thermal stability and share a common, 200 mm focal length, F/1.8 Cassegrain telescope. The optical path is shown in Figure 1, along with examples of spectra recorded by each channel.

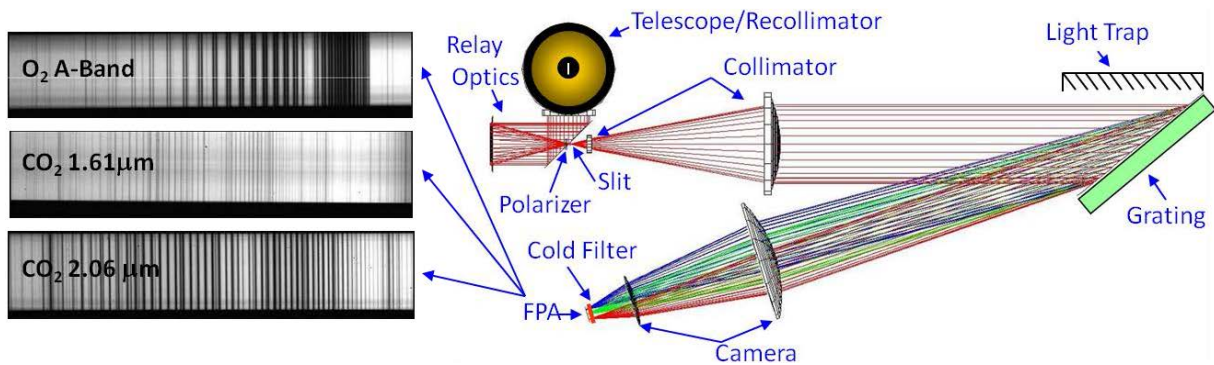


Fig 1. The OCO-2 instrument showing the major optical components and optical path (right) and images of spectra recorded by the Focal plane arrays in the 3 spectral channels (left).

Light entering the telescope is focused at a field stop and then re-collimated before entering a relay optics assembly [6]. It is then directed to one of the 3 spectrometers by dichroic beam splitters, and then transmitted through a narrowband pre-disperser filter. The filter for each spectral range transmits light with wavelengths within $\pm 1\%$ of the central wavelength of the CO_2 or O_2 band and rejects the rest. The light is then refocused onto the spectrometer slits by a reverse Newtonian telescope. Each spectrometer slit is about 3 mm long and 25 μm wide. These long, narrow slits are aligned to produce co-boresighted fields of view that are ~ 0.0005 radians wide by ~ 0.0146 radians long. Because the diffraction gratings efficiently disperse only light that is polarized in the direction perpendicular to the long axis of the slit, a linear polarizer was included in front of the slit to reject the unwanted polarization before it enters the spectrometer, where it could contribute scattered light. Once the light traverses a spectrometer slit, it is collimated by a 2-element collimator, dispersed by a gold-coated, reflective, planar, holographic diffraction grating that works in 1st order. The dispersed light is then focused by a 2-element camera lens onto a 2-dimensional focal plane array (FPA), after traversing a second, narrowband filter just above the FPA, which is cooled to ~ 180 K to reject thermal emission from the instrument.

The spectrometer optics produce a 2-dimensional image of a spectrum on a 1024 by 1024 pixel FPA with 18 μm pixels (Figure 2a). The grating disperses the spectrum onto 1016 of the 1024 FPA columns in the direction perpendicular to the long axis of the slit. The full width at half-maximum (FWHM) of the slit image on the FPA (also called the ‘Instrument Line Shape, or ILS) is sampled by 2 to 3 pixels in the direction of dispersion. The 3 mm long slit limits spatial field of view to only about 190 pixels in the dimension orthogonal to the direction of dispersion. Science measurements are restricted to the center 160 of these 190 pixels.

For normal science operations, the FPAs are continuously read out at 3 Hz. A “rolling readout” method has been adopted for reading out and resetting the FPAs, precluding the need for a physical shutter and eliminating spatial gaps between the exposures. To reduce the downlink data volume and increase the signal to noise ratio, 19-21 adjacent pixels in the FPA dimension parallel to the long axis of the slit (i.e., the spatial direction in Fig. 2) are summed on board to produce up to 8 spatially-averaged spectra along the slit. Each ~20 pixel sum is defined as a “spectral sample.” The angular field of view is defined as by the 1016 spectral samples is defined as a “summed footprint.”

The along-slit angular field of view of each spatially-averaged spectral sample is about 1.8 milliradians (mrad) or 1.3 km at nadir from a 705 km orbit. The angular width of the slit is only 0.14 mrad, but the focus of the entrance telescope was

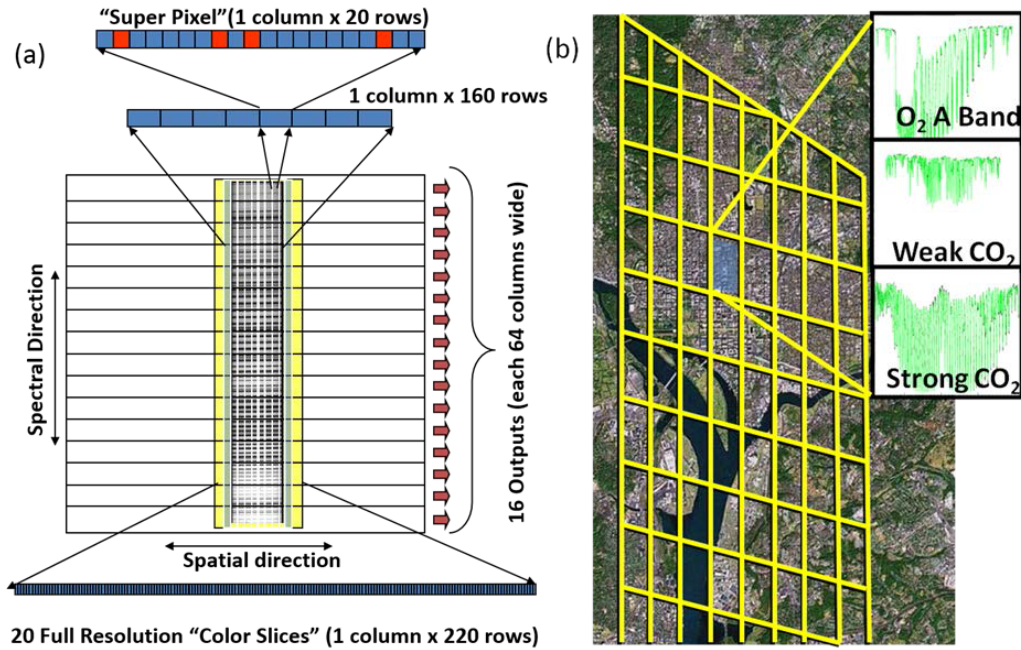


Fig 2. The illumination and readout approach used for the OCO-2 FPAs, showing the direction of spectral dispersion from bottom to top, and the spatial direction from left to right. The ~160 illuminated pixels in the spatial dimension are summed into eight 20-pixel “footprints.” If one or more of the pixels in a footprint is “bad” (red pixels), it is eliminated from the sum. If one or two contiguous pixels in a column are bad, then they are replaced with the average of their good neighbors. If three or more bad pixels are contiguous, then they are replaced with zeros. This algorithm is only applied in the spatial direction—spectral information is never mixed. One of the 20 full-resolution “color slices” is also shown at the bottom. **(b)** Spatial layout of 8 cross-track footprints for nadir observations over Washington, D.C. Each footprint is shaped like a parallelogram, rather than a square, because of the rolling readout of the FPAs and the spacecraft motion.

purposely blurred to increase the effective full width at half maximum of each slit to ~0.5 mrad to simplify the boresight alignment among the 3 spectrometer slits and to further reduce the impact of bad pixels. Because it takes 0.333 seconds to read the 220 active rows of the array and the spacecraft is moving during the rolling readout, the surface footprints are shaped liked parallelograms rather than squares when the slit is oriented orthogonal to the ground track (Figure 2b).

In addition to the 8, spatially-binned, 1016-element spectra, each spectrometer returns up to 20 columns (colors) from each FPA without any on-board spatial binning. These “color slices” sample the full along-slit spatial resolution. Each color slice records a 220-pixel wide region of the FPA that includes the full length of the slit (~190 pixels) as well as a few pixels beyond the ends of the slit [8]. They are used to detect spatial variability within each of the spatially summed spectral samples and to quantify the thermal emission and scattered light within the instrument. The locations of the 20 color slices are specified by commands from the ground.

5. MEASUREMENT APPROACH

OCO-2 flies at the head of the A-Train, in a 98.8 minute orbit that has a 1:36 PM nodal crossing time and a 16-day (233-orbit) ground-track repeat cycle. For routine science operations, the spacecraft points the instrument's bore sight at the local nadir or at the "glint spot," where sunlight is specularly reflected from the Earth's surface. Nadir observations provide the best spatial resolution and yield more useful X_{CO_2} soundings in regions that are partially cloudy, or topographically rough. They also yield more useful data at high latitudes over continents, where the sun is low, surfaces are relatively dark, and the longer optical paths increase the impact of scattering by thin clouds and aerosols. Glint observations have much greater signal-to-noise ratios (SNR) over dark, specular ocean surfaces, and therefore provide more useful X_{CO_2} soundings there. OCO-2 can also target selected surface calibration and validation sites to collect thousands of soundings as the spacecraft flies overhead. The primary surface targets include well calibrated surface sites, such as Railroad Valley, Nevada, and Total Carbon Column Observing Network (TCCON) stations, which make precise measurements of CO_2 and other trace gases from the ground.

Over its first year in orbit, the OCO-2 operations and observing strategy have been optimized to improve the data quality and coverage. For example, the original plan was to maintain the long axis of the slit perpendicular to the "principle plane," defined by the sun, surface footprint, and instrument aperture [6], but this viewing geometry provided too little signal over the ocean near the Brewster angle ($\sim 51^\circ$ for seawater). The instrument boresight (and satellite body) was therefore rotated 30° around the telescope optical axis to increase the signal for glint observations. In the late spring of 2015, the spacecraft's orbit track was adjusted to better align the ground footprints of the nadir OCO-2 soundings with those of the cloud and aerosol soundings from CloudSat and CALIPSO. This modification is expected to provide a larger coincident CloudSat/CALIPSO/OCO-2 data set, for use in validating the OCO-2 cloud and aerosol retrievals. The glint/nadir observing strategy was also modified to produce more regular coverage of the ocean and high latitude continents. The initial strategy acquired only glint or nadir observations over the entire sunlit hemisphere for a complete, 16-day, ground track repeat cycle, and then used the other observing mode in the next 16-day cycle. This approach optimized the coverage of oceans and continents on monthly time scales, but produced 16-day long gaps in the coverage of the ocean while in nadir mode, and limited coverage of high latitude continents while in glint mode. In early July of 2015, this observation strategy was modified to alternate between glint and nadir observations on alternate orbits. This approach yields more continuous coverage of the sunlit hemisphere each day.

6. PRELIMINARY X_{CO_2} RESULTS

The OCO-2 team began delivering calibrated spectral radiance data (Level 1 products) to the Goddard Earth Sciences Data and Information Services Center (GES-DISC) in December 2014 for distribution to the science community. Deliveries of retrieved geophysical quantities including spatially resolved estimates of X_{CO_2} , surface pressure, and solar-induced chlorophyll fluorescence (Level 2 products) to the GES-DISC started in late March 2015. In the summer of 2015, all data collected since routine operations began in early September of 2014 were reprocessed using Version 7 of the OCO-2 algorithm. At the time of writing, these products were being validated to identify and correct regional scale biases.

As the data set has grown over the first year of operations, global maps of X_{CO_2} from OCO-2 started revealing some of the best known features of the atmospheric carbon cycle at unprecedented spatial resolution. In the fall of 2014, as the northern hemisphere biosphere began to slow down and the pole-to-pole gradient in X_{CO_2} almost vanished, CO_2 enhancements from human activities were much more obvious. OCO-2 retrievals showed X_{CO_2} enhancements as large as 1 ppm above the background values co-located with intense fossil fuel emissions in the eastern U.S. and X_{CO_2} enhancements almost twice that large in eastern China. Biomass burning in the Amazon, south-central Africa, and Indonesia also produced X_{CO_2} increases in this range (1-2 ppm) in October. As the season progressed, the X_{CO_2} enhancements associated with biomass burning in Africa move north of the equator.

The largest pole-to-pole gradients in X_{CO_2} were seen in early May of 2015, as land plants in the northern hemisphere were just starting to rapidly absorb CO_2 from the air to form new leaves, branches, and roots (Figure 3). Between mid-May and mid-July, this intense CO_2 drawdown decreased the X_{CO_2} over much of the northern hemisphere by 2% to 3% (8 to 12 ppm out of the ambient 400 ppm background concentration). During this season, X_{CO_2} enhancements co-located with intense fossil fuel combustion and biomass burning were seen in individual OCO-2 ground tracks, but were not readily apparent in the global maps. As noted above, these are some of the most robust features of the global carbon cycle and were expected. As the OCO-2 X_{CO_2} product is validated and the carbon cycle science community continues their analysis

of this growing data set, information on regional-scale sources (emitters) and sinks (absorbers) as well as far more subtle features are expected to emerge.

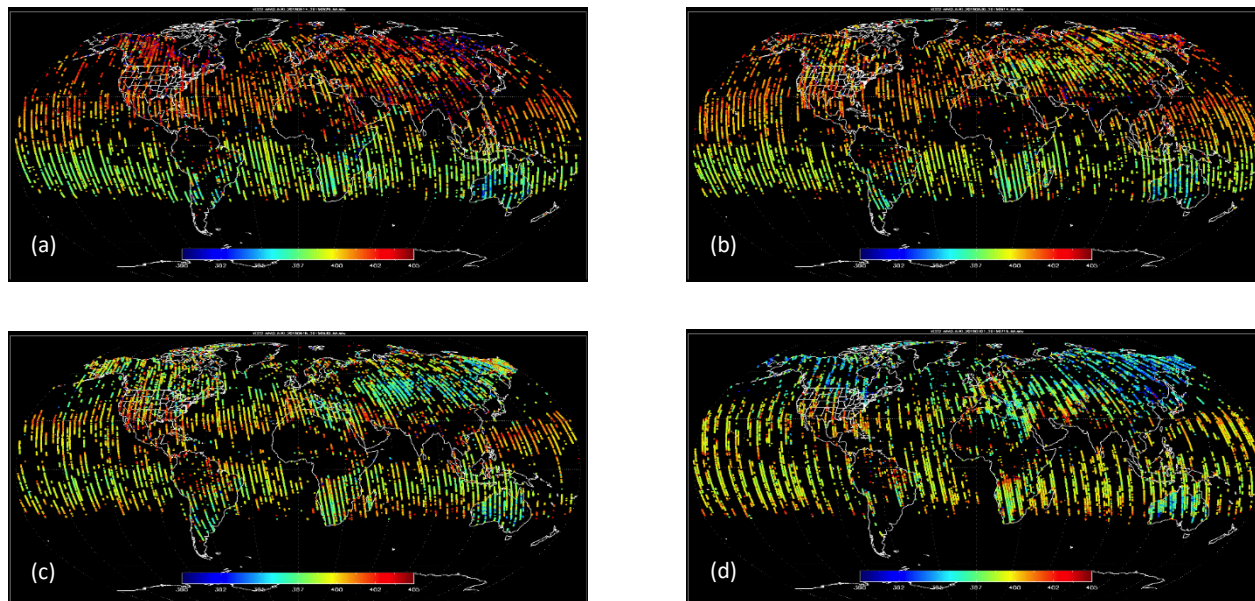


Fig 3. Global maps of X_{CO_2} showing the individual orbit tracks for (a) 14-29 May, (b) 30 May - 14 June, (c) 15-30 June and (d) 1-15 July, produced from OCO-2 observations. The range of latitudes in the southern hemisphere is limited during this season because the sun is near its northernmost latitude. Persistent high clouds near the equator reduce the number of useful soundings there. Large-scale reductions in X_{CO_2} are clearly seen in the northern hemisphere, as the land biosphere rapidly absorbs CO_2 .

7. SUMMARY AND CONCLUSIONS

OCO-2 was successfully launched on July 2, 2014, and two months later began routinely returning almost one million soundings over the sunlit hemisphere each day. On average, about 13% of these soundings are sufficiently cloud free to yield full-column estimates of X_{CO_2} . Nadir soundings over land yield X_{CO_2} estimates with single-sounding random errors of 0.5 - 1 ppm at solar zenith angles less than 60 degrees while ocean glint soundings yield precisions near 0.5 ppm at solar zenith angles less than 70 degrees. Nadir soundings over the ocean and glint soundings over high-latitude land are less precise. Initially, OCO-2 recorded only nadir soundings or glint soundings on alternate, 16-day ground-track repeat cycles. This provided adequate coverage of the globe each month, but produced 16-day gaps in ocean coverage while observing nadir, and similar gaps over high-latitude land while observing glint. In July 2015, this strategy was modified to alternate between glint and nadir soundings on consecutive orbits to yield more continuous coverage each day.

While the X_{CO_2} estimates and other products are being validated to identify and correct biases, global X_{CO_2} maps are starting to reveal some of the best known features of the atmospheric carbon cycle. X_{CO_2} enhancements co-located with intense fossil fuel emissions in eastern U.S. and eastern China are most obvious in the fall, when the north-south X_{CO_2} gradient is small. Enhanced X_{CO_2} coincident with biomass burning in the Amazon, central Africa, and Indonesian is also obvious in the fall. In mid spring, when the north-south X_{CO_2} gradient was largest, these sources were less apparent in global maps. From late May to mid-July, OCO-2 maps show a 2-3% reduction in X_{CO_2} across the northern hemisphere, as the land biosphere rapidly absorbs CO_2 . As the carbon cycle community continues to analyze these OCO-2 data, quantitative estimates of regional-scale emission sources and natural sinks are expected to emerge.

ACKNOWLEDGEMENTS

Part of the research described in this paper was carried out at the Jet Propulsion Laboratory, California Institute of Technology, under a contract with the National Aeronautics and Space Administration.

REFERENCES

- [1] Le Quéré, C., C., Andres, R. J., Boden, T., Conway, T., Houghton, R. A., House, J. I., Marland, G., Peters, G. P., van der Werf, G. R., Ahlström, A., Andrew, R. M., Bopp, L., Canadell, J. G., Ciais, P., Doney, S. C., Enright, C., Friedlingstein, P., Huntingford, C., Jain, A. K., Jourdain, C., Kato, E., Keeling, R. F., Klein Goldewijk, K., Levis, S., Levy, P., Lomas, M., Poulter, B., Raupach, M. R., Schwinger, J., Sitch, S., Stocker, B. D., Viovy, N., Zaehle, S., and Zeng, N., "The global carbon budget 1959–2011." *Earth Syst. Sci. Data*, 5, 165–185 (2013).
- [2] Miller, C. E., D. Crisp, P. L. DeCola, S. C. Olsen, J. T. Randerson, A. M. Michalak, A. Alkhaled, P. Rayner, D. J. Jacob, P. Suntharalingam, D. B. A. Jones, A. S. Denning, M. E. Nicholls, S. C. Doney, S. Pawson, H. Boesch, B. J. Connor, I. Y. Fung, D. O'Brien, R. J. Salawitch, S. P. Sander, B. Sen, P. Tans, G. C. Toon, P. O. Wennberg, S. C. Wofsy, Y. L. Yung, and R. M. Law, "Precision requirements for space-based X_{CO_2} data." *J. Geophys. Res.* 112, D10314 (2007).
- [3] Burrows J. P., Hölzle, E., Goede, A. P. H., Visser, H. and Fricke, W., "SCIAMACHY - Scanning Imaging Absorption Spectrometer for Atmospheric Cartography." *Acta Astronautica*, 35, 445-451 (1995).
- [4] M. Nakajima, A. Kuze, S. Kawakami, K. Shiomi, H. Suto, "Monitoring of the greenhouse gases from space by GOSAT." International Archives of the Photogrammetry, Remote Sensing and Spatial Information Science, XXXVIII, Part 8, JAXA Special Session-5 (2010).
- [5] Crisp, D., R.M. Atlas, F.-M. Breon, L.R. Brown, J.P. Burrows, P. Ciais, B.J. Connor, S.C. Doney, I.Y. Fung, D.J. Jacob, C.E. Miller, D. O'Brien, S. Pawson, J.T. Randerson, P. Rayner, R.J. Salawitch, S.P. Sander, B. Sen, G.L. Stephens, P.P. Tans, G.C. Toon, P.O. Wennberg, S.C. Wofsy, Y.L. Yung, Z. Kuang, B. Chudasama, G. Sprague, B. Weiss, R. Pollock, D. Kenyon, S. Schroll, "The Orbiting Carbon Observatory (OCO) mission." *Advances in Space Research* 34, 700–709 (2004).
- [6] Crisp, D., C. E. Miller, P. L. DeCola, "NASA Orbiting Carbon Observatory: measuring the column averaged carbon dioxide mole fraction from space." *J. Appl. Remote Sens.*, 2, 023508 (2008); doi:10.1117/1.2898457.
- [7] O'Dell, C. W., Connor, B., Bösch, H., O'Brien, D., Frankenberg, C., Castano, R., Christi, M., Crisp, D., Eldering, A., Fisher, B., Gunson, M., McDuffie, J., Miller, C. E., Natraj, V., Oyafuso, F., Polonsky, I., Smyth, M., Taylor, T., Toon, G. C., Wennberg, P. O., and Wunch, D., "The ACOS CO₂ retrieval algorithm – Part 1: Description and validation against synthetic observations." *Atmos. Meas. Tech.*, 5, 99-121 (2012).
- [8] Crisp, D., B. M. Fisher, C. O'Dell, C. Frankenberg, R. Basilio, H. Bösch, L. R. Brown, R. Castano, B. Connor, N. M. Deutscher, A. Eldering, D. Griffith, M. Gunson, A. Kuze, L. Mandrake, J. McDuffie, J. Messerschmidt, C. E. Miller, I. Morino, V. Natraj, J. Notholt, D. M. O'Brien, F. Oyafuso, I. Polonsky, J. Robinson, R. Salawitch, V. Sherlock, M. Smyth, H. Suto, T. E. Taylor, D. R. Thompson, P. O. Wennberg, D. Wunch, and Y. L. Yung, "The ACOS CO₂ retrieval algorithm--Part II: Global X_{CO₂} data characterization." *Atmos. Meas. Tech.*, 5, 687–707 (2012).